Top Catal (2016) 59:497–505
DOI 10.1007/s11244-015-0522-6

ORIGINAL PAPER

Structures and Reactivities of Tin Oxide on Pt(111) Studied by Ambient Pressure X-ray Photoelectron Spectroscopy (APXPS)

Laura Y. Kraya[1] · Guangzhi F. Liu[2,4] · Xiaobo He[1,3] · Bruce E. Koel[1]

Published online: 16 February 2016

Abstract The reduction of disordered and ordered tin oxide monolayers and multilayers on Pt(111) by H_2 was studied in situ by ambient pressure X-ray photoelectron spectroscopy. The disordered tin oxide monolayer was highly reactive and reduced by 5.5×10^{-7} Torr H_2 at 295 K. However, the ordered monolayer was much less reactive, and nearly inert even in 2.2 Torr H_2 at 295 K. Reduction of the tin oxide monolayer occurred only when the sample temperature increased to above 600 K in 5.5×10^{-7} Torr H_2 or when the sample temperature was 450 K in 2.2 Torr H_2. Disordered and ordered multilayers were found to be much less reactive by comparison to the disordered monolayer film. The reduction activity of these ordered and disordered Sn oxide films varied dramatically (by a factor of 10^7), demonstrating the structural flexibility of Sn oxides and the key interplay of structure and reactivity.

Keywords Catalyst · Reduction · Tin Oxide · Photoemission · APXPS

✉ Xiaobo He
xiaobohe2012@gmail.com

Guangzhi F. Liu
frankliu2005@gmail.com

[1] Department of Chemical and Biological Engineering, Princeton University, Princeton, NJ 08544, USA

[2] Department of Chemistry, Lehigh University, Bethlehem, PA 18015-3172, USA

[3] Present Address: 8920 55th Ave. #5G, Elmhurst, NY 11373, USA

[4] Present Address: 1860 Furlow Dr, Redlands, CA 92374, USA

1 Introduction

A fundamental understanding of materials by measuring and correlating electronic structure, geometric structure, and chemisorption properties is essential to interpreting and predicting catalytic reactions [1–4]. It is often found that bimetallic catalysts have improved activity, selectivity, and lifetime compared to their pure counterparts due to the ability of the second metal to produce large perturbations in the electronic structure of the surface allowing the fine tuning of the catalyst's properties for the target reaction [5]. Platinum-tin bimetallic catalysts have a number of important applications in catalysis, including naptha reforming [6, 7], reforming of paraffins [8], hydrogenation/dehydrogenation [9], and also CO oxidation [10–12] and methanol electrooxidation [13–15]. Pt–Sn bimetallic catalysts usually show great improvement in selectivity and lifetime over that of Pt catalysts for these reactions, however the origin of this increase in performance has not been settled. Specifically the role of pure metal and alloy phases, oxidized Sn, and the Pt–SnO_x interface in supported Pt–Sn bimetallic catalysts is not clear [16, 17].

In part due to this issue, oxidation and reduction of bulk Pt–Sn alloys has been studied for a long time [18], along with related studies on Pd-Sn [19], in which oxidation at low temperatures ($T < 500$ K) formed a "quasimetallic" state of Sn with a Sn 3d binding energy less than SnO (Sn^{2+}), and oxidation at higher temperatures leads to an "oxidic" state of SnO_2 (Sn^{4+}). In addition, model catalyst studies of the structure and properties of wetting layers and SnO_2 crystallites in tin-oxide films on Pt(111) single crystal surfaces have been reported [20–25]. At room temperature Sn oxidation leads to amorphous tin-oxide films, and elevated temperatures (above 800 K) lead to a variety of ordered structures in the oxide monolayer. X-ray

photoelectron spectroscopy (XPS) of these tin-oxide films confirmed the existence of three Sn states that have been labeled previously as metallic, ''quasimetallic,'' and oxidic Sn, and furthermore it was concluded that the ''quasimetallic'' state results from oxidized Sn that is still alloyed within the Pt surface layer [25].

The reactivity of these SnO_x/Pt(111) surfaces for CO oxidation has been investigated [7]. In UHV studies, S. Axnanda et al. found that the CO oxidation rate was strongly dependent on the presence of reduced tin oxide sites at the Pt–SnO_x interface. Similar SnO_x nanostructures supported on Pt(111) were probed in situ using ambient pressure XPS (APXPS) and high-pressure scanning tunneling microscopy (STM) to follow the oxidation state and morphology of SnO_x nanoparticles on the SnO_x/Pt(111) surface in the presence of CO gas [26]. It was found that SnO_x nanoparticles are highly reduced, with Sn^{2+} being the dominant oxide species. Under CO gas at 450 K, the Sn^{2+} peak shows a steady decrease and the Sn^0 peak shows a steady increase, with a negligible amount of Sn^{4+} for lower SnO_x coverages. For higher coverages, both Sn^{4+} and Sn^o relative peak ratios sharply increase. No change was observed in the SnO_x nanoparticle shape or density under 0.1 Torr of CO gas. In related studies, in situ APXPS measurements of colloidal PtSn nanoparticle catalysts found that CO oxidation occurred at the interface of Pt and tin oxide domains formed under reaction conditions [27].

The primary objective for the studies reported herein is to provide a clear correlation between structure and reactivity for specific, well-defined tin-oxide surfaces by synthesis of several oxide nanostructures on the Pt(111) surface and utilizing HPXPS (also known as high-pressure photoelectron spectroscopy, HPPES) to obtain XPS data while the sample is exposed to ambient gas pressures up to 2.5 Torr. The reaction investigated is the reduction of the tin oxide surface by hydrogen, and the range of structures studied range from disordered to ordered surfaces in films from monolayer to multilayer thickness. These results will aid in establishing the role that surface structure plays in catalytic reactivity and will help elucidate the role played by Pt in affecting Sn reduction.

2 Experimental Methods

All of the experiments described in this paper were performed in the high pressure photoemission spectroscopy (HPPES) system operated at Beamline 11.0.2 of the advanced light source (ALS) at Lawrence Berkeley National Laboratory (LBL) [28], which is equipped with a differentially pumped electrostatic energy analyzer, low-energy electron diffraction (LEED) optics, an ion sputtering gun for sample cleaning, leak valves and gas dosing lines, and a Sn evaporation doser. The Pt(111) single crystal sample was heated using a ceramic heater that was situated directly beneath the sample. The base pressure in the system was 2×10^{-10} Torr. XPS data were obtained at an X-ray photon energy of 735 eV, with a spot size less than 1 mm and resolution of 0.2–0.4 eV, and no beam damage was observed in control experiments conducted during these investigations.

The Pt(111) single crystal was prepared by a standard procedure consisting of cycles of 500-eV Ar^+ sputtering, annealing at 1000 K in 2×10^{-7} Torr O_2, and finally annealing at 1100 K in UHV. The cleanliness of the sample surface was monitored by XPS. The sample temperature was monitored by a chromel/alumel thermocouple spot welded directly to the side of the Pt(111) crystal. Tin oxide monolayers were prepared using procedures described previously [25]. A $(\sqrt{3} \times \sqrt{3})$R30°-Sn/Pt(111) surface alloy was created by depositing 1-monolayer (ML) Sn on the Pt(111) crystal at 300 K and subsequently annealing to 1000 K for 10 s [29]. This surface was then oxidized by exposure to 4×10^{-8} Torr NO_2 for 40 s at a sample temperature of 400 K. This temperature was chosen to avoid NO adsorption on the surface. No nitrogen contamination of the surface was subsequently detected in XPS. This structure is denoted as the "disordered tin-oxide monolayer", which showed a diffuse LEED pattern with no diffraction spots [25]. Annealing this surface in vacuum to 860 K for 1 min resulted in a (4×4) LEED pattern, corresponding to what we denote here as the "ordered tin-oxide monolayer" structure [25]. Oxidation and annealing of the $(\sqrt{3} \times \sqrt{3})$R30°-Sn/Pt(111) surface alloy 3–5 times resulted in a (5×5) LEED pattern, which results from ordered "nanodots" of SnO_x at the Pt surface. [22] The 2–3 layer disordered oxide film denoted as the "disordered tin-oxide multilayer" was produced by depositing 3-ML Sn in an ambient background gas of NO_2 on the $(\sqrt{3} \times \sqrt{3})$R30°-Sn/Pt(111) surface alloy at 600 K. Annealing this oxide film in vacuum at 900 K for 30 s caused the formation of SnO_2 nanocrystals and an interface layer with a (4×4) LEED pattern, which we will denote herein as the "ordered tin-oxide multilayer" [25].

3 Results and Discussion

3.1 Disordered Tin Oxide Monolayer

The XPS spectrum of a disordered tin-oxide monolayer, as prepared by oxidation of the $(\sqrt{3} \times \sqrt{3})$R30°-Sn/Pt(111) surface alloy at 400 K using NO_2, is shown in Fig. 1. Three components were observed in Sn $3d_{5/2}$ spectra: fully oxidized Sn^{4+} at 486.3 eV, quasimetallic Sn at 485.1 eV, and metallic, alloyed Sn^o at 484.6 eV. The assignment of Sn

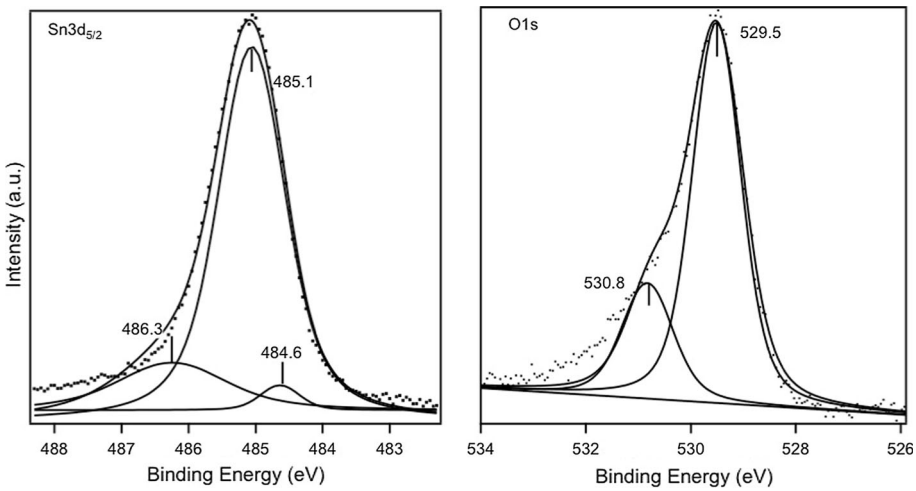

Fig. 1 Sn $3d_{5/2}$ (*left*) and O 1s (*right*) core-level spectra from a disordered tin-oxide monolayer on Pt(111) at 295 K. Decomposition of the *curves* into principal components indicates the presence of primarily a strongly reduced type of tin oxide phase, previously referred to as "quasimetallic" Sn, [25], with small amounts of a more oxidized phase similar to SnO_2, along with a trace of reduced, alloyed Sn

oxidation states corresponding to these peaks has been discussed in previous work [25, 26]. These data show that the disordered tin oxide monolayer is formed by an oxide comprised of nearly all quasimetallic Sn, a state in which Sn is in an oxidation state somewhat below Sn^{2+} and proposed to be Sn that is alloyed with Pt at the surface, but has a Sn–O bond [25]. Consistent with the Sn core levels, Fig. 1 also shows two components for the O 1s spectra: fully oxidized SnO_2 at 530.8 eV and quasimetallic SnO at 529.5 eV.

H_2 reduction of the disordered tin oxide monolayer at 295 K was investigated by collecting both Sn $3d_{5/2}$ and O 1s spectra alternately and continuously during H_2 gas exposure, as shown in Fig. 2. Upon exposure of 5.5×10^{-7} Torr H_2 to the film, the Sn $3d_{5/2}$ peak at 485.1 eV was immediately reduced in height and broadened to lower binding energy. The Sn peak eventually evolved to a narrower peak at 484.6 eV over the course of less than 10 min. This shift in the Sn 3d spectra from 485.1 to 484.6 eV represents a quasimetallic to metallic transition of Sn on the Pt(111) surface. During this reduction process, the O 1s peak decreased in size steadily, but with the quasimetallic component at 529.5 eV more reactive, reducing more quickly, than the SnO_2 component at 530.8 eV. No O 1s signals due to OH or H_2O were detected. An isosbestic point was observed in the XPS spectra, indicating a simple equilibrium between these two species in each case. We note that the disordered oxide monolayer film made from an initial (2×2)-Sn/Pt(111) alloy showed a similar reactivity, i.e., was readily reducible at 295 K (data not shown).

Reduction using the same H_2 pressure (5.5×10^{-7} Torr) was also measured at sample temperatures of 350, 400, and 454 K (not shown). Higher temperatures led to a faster reduction rate. The activation energy of reduction was found to be 8.6 kJ/mol, which was derived from an Arrhenius plot of this data (not shown). This small

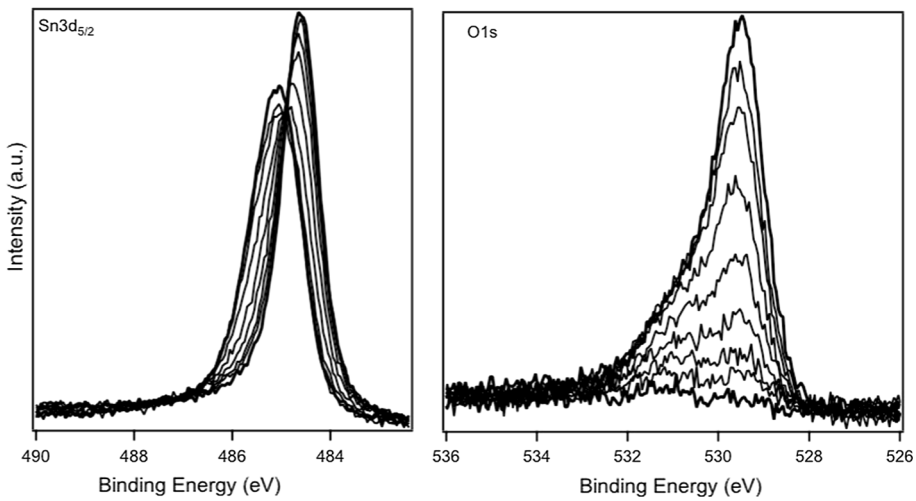

Fig. 2 Sequence of Sn $3d_{5/2}$ (*left*) and O 1s (*right*) XPS spectra obtained during reduction of a disordered oxide monolayer using 5.5×10^{-7} Torr H_2 at 295 K. *Top bolded curves* were obtained prior to H_2 exposure. *Bottom bolded curves* were obtained after H_2 exposure of 571s. Other curves were collected after H_2 exposure of 10, 57, 113, 170, 227, 284, and 340 s, respectively

activation energy indicates a very reactive and easily reducible SnO_x surface at room temperature.

3.2 Ordered Oxide Monolayers

As reported previously [25], LEED and STM show a disordered oxide film below 800 K. Annealing in vacuum orders the tin oxide adlayer such that LEED spots appear at 840 K and eventually forms a "diamond necklace" pattern and subsequently a (4x4) pattern with increasing temperature. This transition from a disordered monolayer to an ordered monolayer causes the Sn $3d_{5/2}$ peak to shift (not shown) from 485.0 to 484.8 eV, which indicates that Sn was reduced to some degree during the transition. Concomitantly, the O 1s peak shifted from 529.5 to 529.3 eV and decreased in size. Some oxygen desorbs during the annealing, but this causes only small changes in XPS. Larger changes in XPS, and huge changes in the reactivity of the film, are observed for the formation of the specific ordered monolayer structures discussed below, and thus are associated with the loss of highly reactive species or sites during annealing.

Specific reduction experiments were carried out on the (4 × 4) ordered oxide monolayer, which was prepared by annealing the disordered monolayer film at 860 K for 1 min. No reduction occurred upon exposure to 5.5×10^{-7} Torr H_2 at 295 K, and the ordered monolayer was inert even in 2.2 Torr H_2 at 295 K. Reduction of the SnO_x film happened only when the sample temperature increased to 450 K in 2.2 Torr H_2, as shown in Fig. 3 (or when the sample temperature reached to 630 K in 5.5×10^{-7} Torr H_2 as shown later in Fig. 4). In Fig. 3, the top curves for Sn $3d_{5/2}$ and O 1s spectra were collected at 530 K in 5.5×10^{-7} Torr H_2, and these showed no change compared to those prior to H_2 exposure. Curve fitting shows that this ordered monolayer has an increased contribution from metallic tin, as described above. The bottom panels show that reduction in 2.2 Torr H_2 carried out over a 15 min period at a sample temperature of 450 K caused a shift in the Sn $3d_{5/2}$ peak from 484.8 to 484.6 eV and eliminated the O 1s peak at 529.5 eV. Reduction leads to formation of fully reduced metallic Sn species, however, the appearance of a shoulder around 484.0 eV may indicate that there are small binding energy differences between different forms of this Sn, for example surface and subsurface alloyed Sn as well as non-alloyed Sn.

In Fig. 4, the curves for Sn $3d_{5/2}$ and O 1s spectra were collected at 295 K in 5.5×10^{-7} Torr H_2, and these showed no change compared to those prior to H_2 exposure. Reduction did occur when the sample temperature was increased to ~630 K. During reduction over a 5 min period, the Sn $3d_{5/2}$ peak shifted from 484.8 eV to 484.6 eV, and the O 1s peak at 529.3 eV decreased in intensity, i.e. the amount of metallic tin increased and the amount of quasimetallic tin decreased. Following reduction under these conditions, some small amount of SnO_2 and OH groups remain at the surface.

A different ordered oxide monolayer can be formed. Upon oxidation and annealing of the $(\sqrt{3} \times \sqrt{3})$R30°-Sn/Pt(111) alloy 3–5 times, a (5 × 5) LEED pattern results. Previous STM studies reveal that oxidation of the surface forms dense, regular, oxide-island arrays, i.e. ordered "nanodots" of SnO_x at the Pt surface [22]. There are large interfacial areas available for the oxide nanodots, and the large crevices and packing defects may give reactants access to the underlying Pt and/or Pt–Sn alloy surface. The top panels in Fig. 5 shows the core level spectra obtained from the (5 × 5) ordered tin-oxide monolayer surface prior to H_2 exposure. The Sn $3d_{5/2}$ spectrum has peaks at 484.5 and 486.2 eV and the O 1s spectrum has a peak at 529.9 eV. These spectra can be decomposed into peaks that indicate the surface contains a substantial amount of SnO_2, less of the quasimetallic tin oxide state, and a larger component of reduced Sn compared to the (4 × 4) structure investigated above. The bottom panels show the spectra obtained during reduction at 520 K using 2.1 Torr H_2 over a 10 min period. These conditions were sufficient to fully reduce the surface, eliminating any oxidized Sn species and removing any OH species. The (5 × 5) "nanodot" surface structure is thus less reactive than that of the (4 × 4) monolayer (requiring 2.1 Torr H_2 at 520 K for 10 min vs. 2.2 Torr H_2 at 450 K for 5 min) and this difference can be ascribed at least in part to the increased amount of SnO_2 present for the (5 × 5) monolayer film. Importantly, both of the ordered tin-oxide monolayers were found to be dramatically less reactive than the disordered monolayer.

3.3 Disordered 2–3 Layer Oxide Film

A disordered oxide multilayer film was prepared by depositing 3-ML Sn on the Pt(111) crystal at 600 K in a background of NO_2. Initially, prior to reduction, Fig. 6 (top left) and (top right) shows that two components are present at 486.1 and 485.3 eV for the Sn $3d_{5/2}$ peaks and 529.6 and 530.7 eV for the O 1s peaks. This represents a nearly fully oxidized amorphous SnO_2 film, where the oxide layer is thick enough to block photoemission from the metallic substrate. This multilayer was much less reactive than the disordered oxide monolayer film. Reduction of this film occurred readily in 2.5 Torr H_2 only when the sample temperature was increased to 625 K. Figure 6(bottom left) and (bottom right) provides core-level spectra obtained during reduction of this disordered oxide multilayer film during exposure to 2.5 Torr H_2 at 625 K obtained over a 10 min period. As shown in Fig. 6(bottom left), the Sn $3d_{5/}$

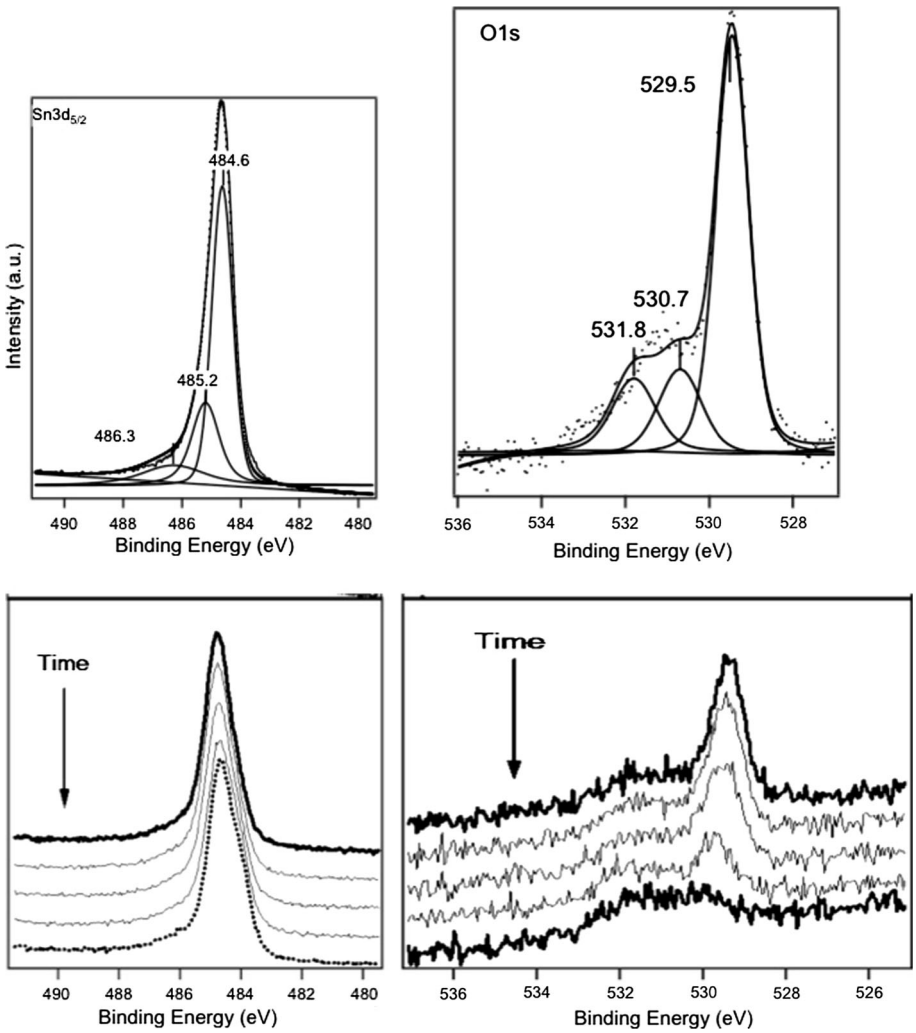

Fig. 3 *Top panels* Sn $3d_{5/2}$ (*left*) and O 1s (*right*) core-level spectra from an ordered tin-oxide monolayer on Pt(111) obtained by annealing the disordered film at 860 K for 1 min. Spectra were obtained at 530 K. Decomposition of the *curves* into principal components indicates a large increase in the contribution of metallic Sn as well as the presence of a strongly reduced type of tin oxide phase, previously referred to as "quasimetallic" Sn, [25], with little SnO_2 phase, compared to that in Fig. 1. *Bottom panels* Sequences of Sn $3d_{5/2}$ and O 1s core-level spectra obtained during reduction of this ordered tin oxide monolayer on Pt(111) at 450 K in the presence of 2.2 Torr H_2. The *top bolded curves* were obtained at a temperature of 530 K. Other *curves* shown were obtained after H_2 exposures of 57, 113, 170, and 227 s

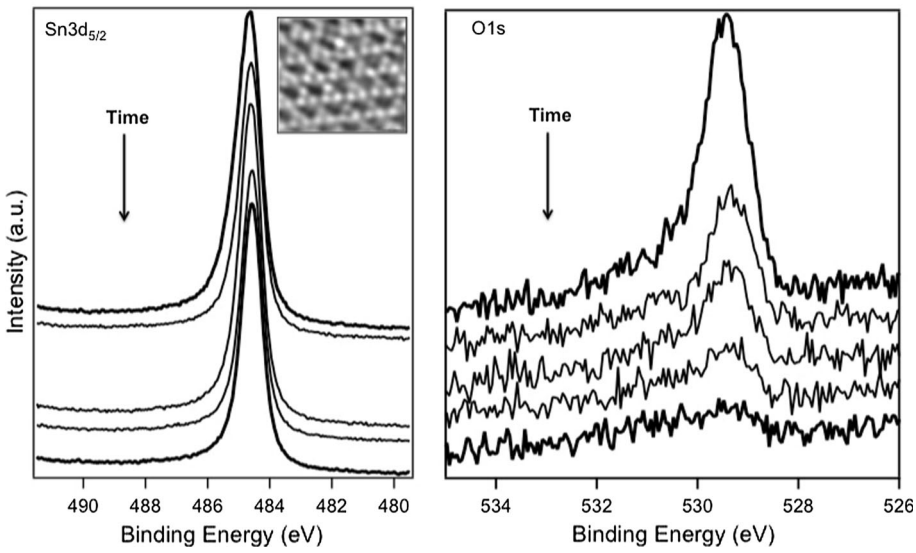

Fig. 4 Sequence of Sn $3d_{5/2}$ and O 1s core-level spectra obtained during reduction of a (4×4) ordered oxide monolayer using 5.5×10^{-7} Torr H_2 at 630 K. The *top curves* were obtained at 530 K and the *lower curves* were obtained sequentially during reduction at 630 K at 57, 113, 170, and 227 s, respectively

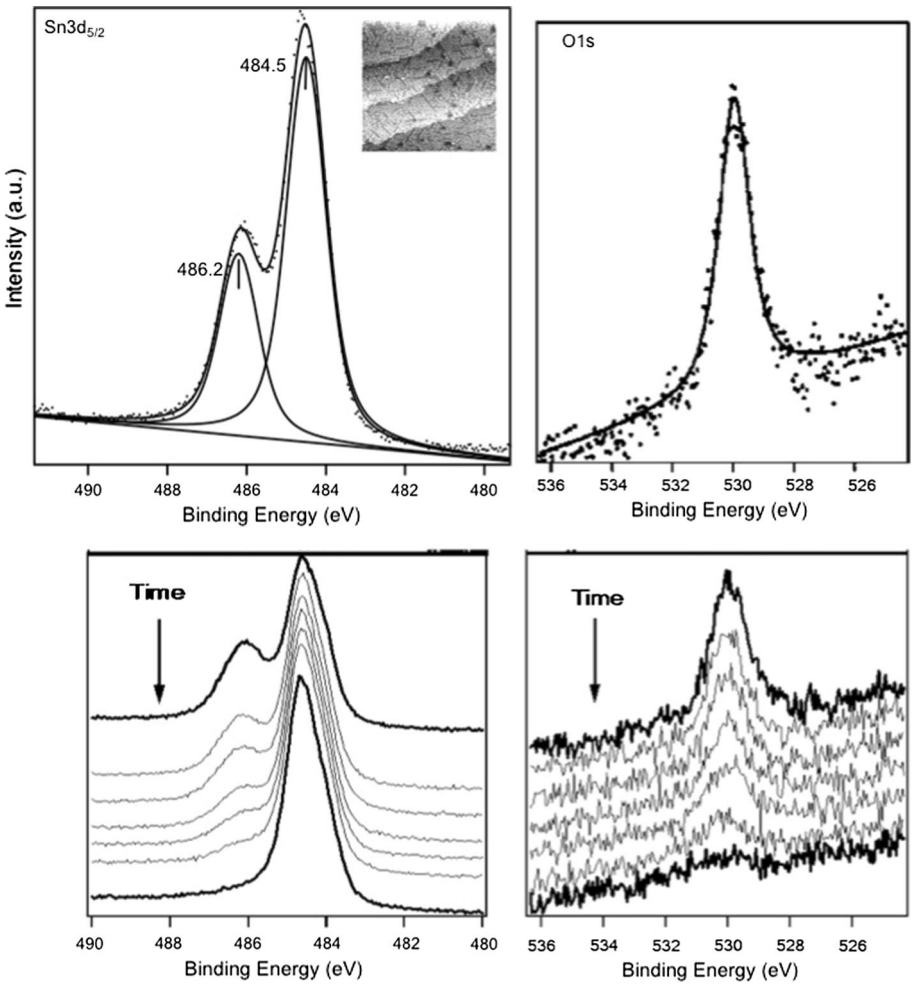

Fig. 5 Top panels: Sn $3d_{5/2}$ (*left*) and O 1s (*right*) core-level spectra from a (5 × 5) ordered oxide monolayer on Pt(111) at 295 K. Decomposition of the *curves* into principal components indicates the presence of primarily a strongly reduced type of tin oxide phase, previously referred to as "metallic" Sn, along with a large amount of reduced, alloyed Sn. *Bottom panels* Sequence of Sn $3d_{5/2}$ and O 1s core-level spectra obtained during reduction of a (5 × 5) ordered oxide monolayer using 2.1 Torr H_2. The *top bold curves* were obtained at 295 K, and the *curves below* were obtained sequentially during reduction at 520 K at 57, 113, 170, and 227 s, respectively

$_2$ peak decreased in intensity and shifted to lower binding energy during the reduction process. The O 1s peak, as shown in Fig. 6(bottom right), decreased in intensity at a constant peak position during reduction under these conditions.

3.4 Ordered 2–3 Layer Oxide Film

Upon annealing a disordered oxide multilayer (as prepared above) to 900 K for 30 s, a 2–3 layer oxide film giving a (4 × 4) LEED pattern was produced. Core-level spectra for this film prior to reduction are shown in Fig. 7(top left) and (top right), along with an STM image obtained under similar conditions by Batzill et al. [21, 22] to give a qualitative picture of the film. The image displayed protrusions separated by twice the Pt(111) surface lattice constant, where every second protrusion in every second row was missing. These protrusions were attributed to SnO 'pseudomolecules'. The Sn $3d_{5/2}$ core level spectr has a peak at 486.3 eV due to the SnO_2 crystallites, a peak at 484.6 eV due to reduced Sn species in the (4 × 4) adlayer lattice and alloyed Sn, and a very small peak at 485.1 eV. The O 1s peak can be decomposed into two components at 530.8 eV also indicates a large signal from the SnO_2 crystallites and the peak at 529.9 eV indicates a smaller contribution from the reduced oxide species in the (4 × 4) adlayer lattice. Both the Sn $3d_{5/2}$ peak at 486.3 eV and the O 1s peak at 530.8 eV have slightly higher binding energies than that for the disordered multilayer perhaps because this annealing treatment forms fully oxidized SnO_2 crystals.

This ordered multilayer film was more reactive than the disordered multilayer film by about a factor of two. Figure 7(bottom left) and (bottom right) provides APXPS spectra obtained during reduction of this (4 × 4) ordered multilayer oxide film at 600 K during exposure to 1.9 Torr H_2 obtained over a 6 min period. During reduction of this film, the Sn $3d_{5/2}$ peak at 486.3 disappears, leaving a single peak at 484.6, as shown in Fig. 7(bottom left). The O 1s peak at 530.8 eV was eliminated without any shift.

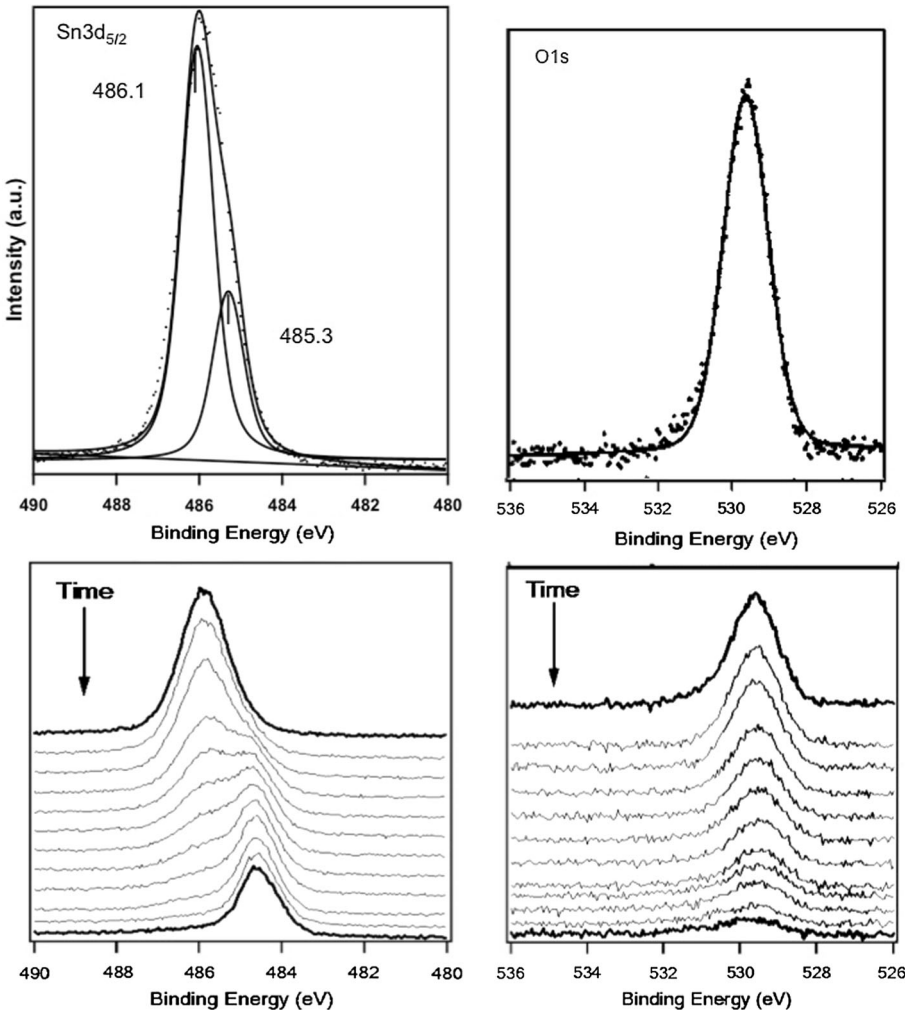

Fig. 6 *Top panels* Sn $3d_{5/2}$ (*left*) and O 1s (*right*) core-level spectra from a disordered oxide multilayer film on Pt(111) at 295 K. *Bottom panels* Sequence of Sn $3d_{5/2}$ and O 1s core-level spectra obtained during reduction of a disordered oxide multilayer film using 2.5 Torr H_2. The *top bold curves* were obtained at 295 K, and the subsequent *curves* were obtained sequentially during the reduction at 625 K

3.5 Comparison of Tin Oxide Films on Pt(111) Surfaces

APXPS spectra of hydrogen reduction of tin oxides on Pt(111) show that the disordered monolayer is 10^7 times more reactive than the ordered (4 × 4) monolayer produced by annealing in vacuum prior to reduction. As we discussed, annealing in vacuum from 328 to 872 K to enable the transition from a disordered to ordered tin oxide monolayer causes some oxygen to be desorbed during the annealing, but this reduction causes only small changes in the Sn $3d_{5/2}$ and O 1s XPS spectra. Thus, determination of the origin of this high reactivity awaits further study, but we can conjecture that it is due to the presence of defects and vacancies in the disordered tin oxide film that are very reactive species or special sites, and these are removed during the formation of ordered monolayer produced at high temperatures. Consistent with such an explanation is the lack of evidence for a long induction time observed for well-ordered oxide films in many cases (except for the film in Fig. 7, which contains well-ordered SnO_2 nanocrystallites). Further oxidation and annealing treatments that convert the ordered (4 × 4) oxide monolayer can produce an ordered (5 × 5) nanodot monolayer structure, but this was found to be less reactive than the (4 × 4) monolayer. This also might be expected due to the higher concentration of fully oxidized SnO_2 component.

The disordered monolayer tin oxide film is also dramatically more reactive for hydrogen reduction than the disordered multilayer tin oxide films. Thus, it is not only the disordered nature of the tin oxide film that controls reactivity. This higher reactivity of the disordered monolayer tin oxide film compared to disordered multilayer films can be attributed to the reduced Sn species that characterize the "quasimetallic" nature of both the ordered and disordered monolayers. Electronic effects due to bonding at the interface are expected since the Pt–Sn bond involves charge transfer from Sn to Pt atoms and rehybridization in Pt atoms that localize electrons in the region between the metal centers [30]. The large decrease in

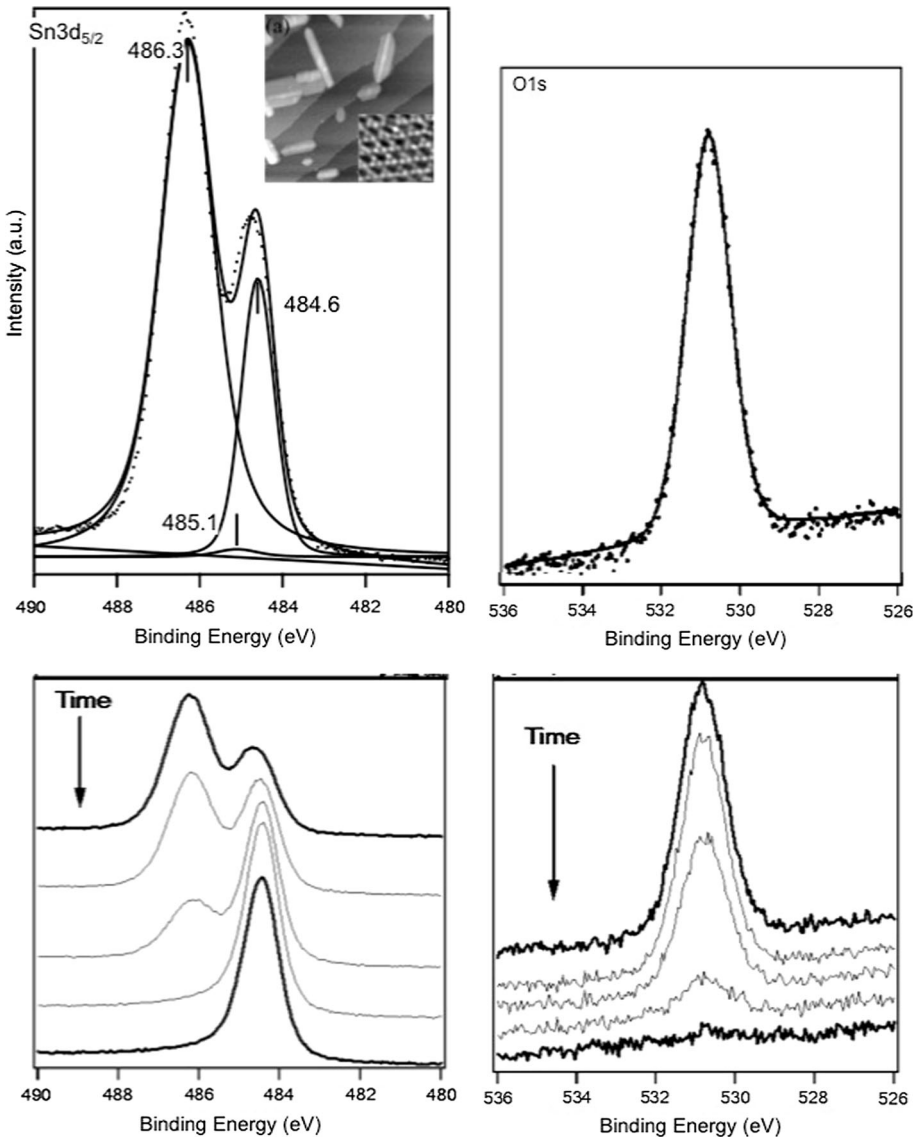

Fig. 7 *Top panels* Sn $3d_{5/2}$ (*left*) and O 1s (*right*) core-level spectra from a (4 × 4) ordered oxide multilayer film on Pt(111) at 295 K. *Bottom panels* Sequence of Sn $3d_{5/2}$ and O 1s core-level spectra obtained during reduction of a (4 × 4) ordered oxide multilayer film using 1.9 Torr H_2. The *top bold curves* were obtained at 295 K, and the *curves below* were obtained sequentially during reduction at 600 K

reactivity that occurs after growth of a disordered tin oxide multilayer film on top of the disordered monolayer can be attributed to formation of a tin oxide film that is composed much more extensively of SnO_2 and a reduced influence of the reactive quasimetallic Sn.

The mechanism for reducing these oxide films by hydrogen involves several elementary steps, including importantly hydrogen dissociation, water formation, and water desorption, but the detailed reaction mechanism and the rate determining step is not known and could easily depend on the oxide film structure. A better understanding of this chemistry and the rates for the elementary steps involved would be helpful to explain the origin of the large changes in reactivity we observed. For example, it would be important to understand the ability of each of these film structures to dissociate hydrogen. This information is not known and will need to come from future additional studies.

4 Conclusions

We have shown that even for this model study using ultrathin films of tin oxide on a Pt(111) single crystal substrate, the Pt–SnO_x interface is characterized by a variety of structures that illustrate the complexity of metal/oxide interfaces and difficulties in modeling and predicting the structure and reactivity of such interfaces. These Sn-oxide nanostructures have different chemical and electronic properties that may be important to existing devices/catalysts and future developments of heterogeneous catalysts, electrocatalysts, and sensors. We find

enormous sensitivity of the reduction of these tin oxide films on the detailed chemical nature and structure of the films. Such sensitivity can alter the thermal reduction temperature by 300 K and the reducibility in H_2 by many orders of magnitude. For example, a disordered tin oxide monolayer is reduced at 300 K by 6×10^{-7} Torr H_2 in 10 min, while the ordered (4×4) monolayer is only reduced at 450 K in 2.2 Torr H_2 in 5 min, more than a factor of 10^7 difference in reactivity.

Acknowledgments BEK acknowledges that this material is based upon work supported by the National Science Foundation under Grant No. CBET-1264737. The authors would like to acknowledge H. Bluhm at LBL National Lab for his contribution to the experimental section of this work.

References

1. Somorjai GA, Li Y (2010) Introduction to surface chemistry and catalysis. Wiley, Hoboken
2. Yu W, Porosoff M, Chen J (2012) Review of Pt-based bimetallic catalysts: from model surfaces to supported catalysts. Chem Rev 112:5780–5817
3. Kraya LY, Kraya R (2013) Polarization dependence of molecular adsorption on ferroelectrics. Acta Crystallogr Sect B B69:105–109
4. Zhou W, An W, Su D, Palermo R, Liu P, White M, Adzic R (2012) Electrooxidation of methanol at SnO_x-Pt interface: a tunable activity of tin oxide nanoparticles. J Phys Chem Lett 3:3286–3290
5. Rodriguez J, Goodman D (1992) The nature of the metal-metal bond in bimetallic surfaces. Science 257(5072):897–903
6. Rahimpour M, Jafari M, Iranshahi D (2013) Progress in catalytic naptha reforming process: a review. Appl Energy 109:79–93
7. Axnanda S, Zhou WP, White MC (2012) CO oxidation on nanostructured SnO_x/Pt(111) surfaces: unique properties of reduced SnO_x. Phys Chem Chem Phys 14:10207–10214
8. Bentahar FZ, Candy JP, Basset JM, Le Peltier F, Didillon B (2001) Surface organometallic chemistry on metal in water: chemical modification of platinum catalyst surface reaction with hydrosoluble organotin complexes: application to the selective dehydrogenation of isobutane to isobutane. Catal Today 66(2–4):303–308
9. Cortright RD, Dumesic JA (1995) Effects of potassium on silica-supported Pt and Pt/Sn catalysts for isobutane dehydrogenation. J Catal 157:576
10. Schubert MM, Kahlich MJ, Feldmeyer G, Huttner M, Hackenberg S, Gasteiger HA, Behm RJ (2001) Bimetallic Pt-Sn catalyst for selective CO oxidation in H_2-rich gases at low temperature. Phys Chem Chem Phys 3:1123–1131
11. Morimoto Y, Yeager E (1998) CO oxidation on smooth and high area Pt, Pt-Ru, and Pt-Sn electrodes. J Electroanal Chem 441(1–2):77–81
12. Hayden B, Rendall M, South O (2003) Electro-oxidation of carbon monoxide on well-ordered Pt(111)/Sn surface alloys. J Am Chem Soc 125(25):7738–7742
13. Gokagac G, Kennedy B, Cashion J, Brown LJ (1993) Characterization of carbon supported Pt-Sn bimetallic catalysts for the electrochemical oxidation of methanol. J Chem Soc Faraday Trans 89:151–157
14. Arico AS, Antonucci V, Giordano N (1994) Methanol oxidation on carbon-supported platinum-tim electrodes in sulfuric acid. J Power Sources 50(3):295–309
15. Knani S, Chirchi L, Baranton S, Napporn T, Leger J-M, Ghorbel A (2014) A methanol—tolerant carbon supported Pt-Sn cathode catalysts. Int J Hydrogen Energy 39(17):9070–9079
16. Antos GJ, Aitani A (2004) Catalytic naptha reforming, revised and expanded. CRC Press, Boca Raton
17. Vigne F, Haubrich J, Loffreda D, Sautet P, Delbecq F (2010) Highly selective hydrogenatio of butadiene on Pt/Sn alloy elucidated by first-principles calculations. J Catal 275(1):129–139
18. Asbury DA, Hoflund GB (1988) The influence of annealing and low-pressure oxygen exposure on a sputtered Pt_3Sn alloy surface. Surf Sci 199:552–566
19. Rotermund HH, Penka V, De Louise LA, Brundle CR (1987) Oxygen interaction with Pd_3Sn: X-ray photoelectron spectroscopy and secondary ion mass spectrometry. J Vac Sci Technol A 5:1198
20. Saliba N, Tsai Y, Koel B (1999) Oxidation of ordered Sn/Pt(111) surface alloys and thermal stability of the oxides formed. J Phys Chem B 103:1532–1541
21. Batzill M, Beck D, Koel B (2001) Structure of monolayer tin oxide films on Pt(111) formed using NO_2 as an efficient oxidant. Phys Rev B 64:245402
22. Batzill M, Beck DE, Koel BE (2001) Self-organized molecular-sized hexagonally ordered SnO_x nanodot superlattices on Pt(111). Appl Phys Lett 78:2766–2768
23. Batzill M, Beck D, Jerdev D, Koel B (2001) Tin-oxide overlayer formation by oxidation of Pt-Sn(111) surface alloys. J Vac Sci Technol A 4:1953
24. Batzill M, Beck D, Koel B (2004) Metastable surface structures of the bimetallic Sn/Pt(100) system. Surf Sci 558:35–48
25. Batzill M, Kim J, Beck D, Koel B (2004) Epitaxial growth of tin oxide on Pt(111): structure and properties of wetting layers and SnO_2 crystallites. Phys Rev B 69:165403
26. Axnanda S, Zhu Z, Zhou W, Mao B, Chang R, Rani S, Crumlin E, Somorjai G, Liu Z (2014) In situ characterizations of nanostructured SnO_x/Pt(111) surfaces using ambient-pressure XPS (APXPS) and high-pressure scanning tunneling microscopy (HPSTM). J Phys Chem C 118:1935–1943
27. Michalak W, Krier J, Alayoglu S, Shin J, An K, Komvopoulos K, Liu Z, Somorjai G (2013) CO oxidation on PtSn nanoparticle catalysts occurs at the interface of Pt and Sn oxide domains formed under reaction conditions. J Catal 312:17–25
28. Bluhm H, Andersson K, Araki T, Benzerara K, Brown GE, Dynes JJ, Ghosal S, Gilles MK, Hansen HC, Hemminger JC (2006) Soft X-ray microscopy and spectroscopy at the molecular environmental science beamline at the advanced light source. J Electron Spectrosc Relat Phenom 150:86–104
29. Paffett MT, Windham RG (1989) Surface modification of Pt(111) by Sn adatoms: evidence for the formation of ordered overlayers and the surface alloys. Surf Sci 208:34–54
30. Rodriguez JA, Jirsak T, Chaturvedi S, Hrbek J (1998) Surface chemistry of SnO_2 on Sn and Sn/Pt(111) alloys: effects of metal-metal bonding on reactivity towards sulfur. J Am Chem Soc 120:11149–11157